Accepted Manuscript

Title: Experimental and theoretical investigations of Cs$^+$ adsorption on crown ethers modified magnetic adsorbent

Authors: Zhong Liu, Yongquan Zhou, Min Guo, Baoliang Lv, Zhijian Wu, Wuzong Zhou

Please cite this article as: Liu Z, Zhou Y, Guo M, Lv B, Wu Z, Zhou W, Experimental and theoretical investigations of Cs$^+$ adsorption on crown ethers modified magnetic adsorbent, *Journal of Hazardous Materials* (2019), https://doi.org/10.1016/j.jhazmat.2019.03.022

Experimental and theoretical investigations of Cs⁺ adsorption on crown ethers modified magnetic adsorbent

Zhong Liu[a,b], Yongquan Zhou[a,b], Min Guo[a,b], Baoliang Lv*[c], Zhijian Wu[a,b], Wuzong Zhou*[d]

[a] *Key Laboratory of Comprehensive and Highly Efficient Utilization of Salt Lake Resources, Qinghai Institute of Salt Lakes, Chinese Academy of Sciences, Xining. 810008, China.*

[b] *Key Laboratory of Salt Lake Resources Chemistry of Qinghai Province, Xining 810008, China.*

[c] *State Key Laboratory of Coal Conversion, Institute of Coal Chemistry, Chinese Academy of Sciences, Taiyuan 030001, China. lvl604@sxicc.ac.cn*

[d] *EaStCHEM, School of Chemistry, University of St Andrews, St Andrews, Fife KY16 9ST, UK, Telephone: +44 1334 467276, Fax: +44 1334 463808, E-mail: wzhou@st-andrews.ac.uk*

Graphical Abstract

Ms. Ref. No.:   HAZMAT-D-18-05778
Title: Experimental and theoretical investigations of Cs+ adsorption on crown ethers modified magnetic adsorbent

Highlights

- A bifunctional absorbent for Cs^+: Fe_3O_4@18-Crown-6 ether is developed.

- The adsorbent has a superparamagnetic property, allowing an easy recycling.

- The adsorbent has a high capacity and high selectivity of Cs^+ adsorption.

- The experimental results are supported by the DFT calculations.

Abstract

Carboxyl Fe_3O_4 nanoparticles (Fe_3O_4@R−COOH) modified with 18-Crown-6 ether functional groups have been prepared via an amidation reaction and used as bifunctional adsorbent for Cs^+. The adsorbent has a superparamagnetic property, allowing an easy recycling, and a high capacity of Cs^+ adsorption on the crown ether. The adsorption isotherms and kinetic behaviors agree well with the Langmuir and the pseudo-second-order models. The material exhibits a high selectivity for Cs^+ in the solution with co-existing cations (NH_4^+, Rb^+, K^+, Na^+ and Li^+). A theoretical calculation according to density functional theory (DFT) is used to estimate the structure of Cs^+ adsorption on crown ether, demonstrating an exothermic process and showing a good agreement with the experimental observations. The adsorption behavior is affected not only by the size of macrocyclic crown ethers, but also by the chelating symmetry and the binding energy. The newly developed adsorbent has a potential application for removing cesium out of wastewater and salt lakes.

Keywords: carboxyl Fe_3O_4; magnetic adsorbent; crown ethers; cesium; adsorption.

1. Introduction

Among a large mumber of toxic contaminants, ^{137}Cs is one of the most harmful isotopes with a high fission yield of ~6.15%, 30 years half-life, strong γ radiation, and a high solubility in water [1]. The damage of the Fukushima Daiichi Nuclear Power Plant by an earthquake resulted in the release of highly harmful radionuclides, including a significant amount of radioactive cesium, into the environment [2]. Therefore, development of better methods for separating cesium from radioactive wastewater is highly demanded. A variety of separation methods have been studied, including solvent extraction [3], ion-exchange [4], precipitation [5] and adsorption [6]. Among them, the adsorption technique is most promising because of its low cost and environment-friendly, especially at a low concentration of the target ions in wastewater. But it is still a challenge to design and fabricate sorbents with the properties of fast recycling and a high selectivity.

In order to quickly separate the adsorbents from water after adsorption of target ions, the magnetic separation method has an advantage in the recovery without filtration and centrifugation. For example, potassium nickel hexacyanoferrate coated on magnetite surface has been made to apply in the collection of low-level cesium from liquid radioactive waste [7]. Prussian-blue-modified magnetite for treatment of Cs^+ in water was also tried [8]. However, the previously reported magnetic adsorbents coated with zeolites [9], polyoxometalates [10], multivalent phosphates [11], titanium ferrocyanide and hexacyanoferrates [12,13] normally do not have a high selectity of Cs^+ when it co-exists with other alkali cations [14].

On the other hand, as good ionophores, crown ethers form a class of compounds for binding certain alkali cations in solution. For example, Awual et al. clarified that the mesoporous silica monoliths modified with dibenzo-18-Crown-6 ether had a high selectivity of Cs^+ when Na^+ and K^+ ions co-exist [15]. Furthermore, the 18-Crown-6 ether can be prepeared as an indicator electrode for detecting Cs^+ in spiked tap water due to its high selectivity property [16]. 18-Crown-6 ether can also be a candidate of extracting agent with high efficiency and high selectivity for Cs^+ in industry [17,18]. But as a macrocyclic ligand, large scale application of 18-Crown-6 ether in solvent extraction is restricted by high cost of chemicals and environmental pollution [19].

3

Consequently, it is urgently needed to develop new adsorbents with a combination of properties of magnetic separation and high adsorption/selectivity for extracting Cs^+ from solutions.

In this work, a high selectivity and low-cost adsorbent for Cs^+ was fabricated by grafting 18-Crown-6 ether onto superparamagnetic Fe_3O_4 nanoparticles. The structures of the nanocomposites were studied by using various techniques including X-ray diffraction (XRD), scanning electron microscopy (SEM) and transmission electron microscopy (TEM). The adsorption behavior of the specimens was studied by simulating the adsorption kinetics curve and adsorption isotherm. By using density functional theory (DFT), we also calculated the chelating positions of the captured Cs^+ cations, and understood the origin of the high selectivity.

2. Materials and methods

2.1. Preparation of adsorbents

All the chemical reagents were purchased from China National Medicines Company (Beijing China) with analytical reagent grade. 0.02 mol $FeSO_4 \cdot (NH_4)_2SO_4 \cdot 6H_2O$ was added into 120 mL water to form a Fe precursor solution. 10 mL of oleic acid (R–COOH), 2 g NaOH and 30 mL ethanol were mixed under stirring for 30 min, to which was added the Fe precursor solution. A precipitate appeared after further stirring for about 2 min. Finally, after keeping stirring for 15 min, the mixed reactants were transferred into a 200 mL telfon-lined autoclave and maintained at 180 °C in an oven for 24 h, then cooled to room temperature. The powder product was recovered by washing with ethanol and dimethylformamide (DMF) for three times. We expect the product at this stage contains Fe_3O_4 nanocrystals with a surface coating of oleic acid, designated Fe_3O_4@R–COOH [20] (Fig. 1).
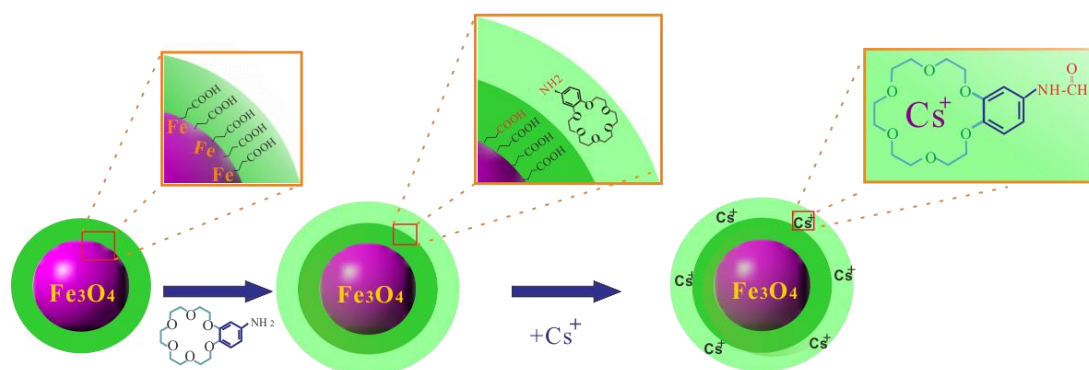
Fig. 1. Proposed formation procedure of magnetic adsorbent and adsorption process of Cs^+ on the particle surface.

The Fe_3O_4@R−COOH particles were gathered by a magnet and then re-dispersed in 200 mL DMF with 0.02 g 1-(3-Dimethylaminopropyl)-3-ethylcarbodiimide hydrochloride (EDCI) and 0.014 g 1-Hydroxybenzotriazole hydrate (HOBT) in a 400 ml three nech flask, preventing the −COOH functional groups from self-dehydration/combination during the later reaction with ethers. After stirring with 400 rpm for 1 h, 0.042 mL N,N-Diisopropylethylamine (DIEA) as a dehydrating agent and 0.2 g 4'-Aminobenzo-18-Crown-6 were added into the solution under stiring for 6 h. Dehydration would take place in between −COOH of the acid and −NH_2 of the ether, linking them together to form new organic functional groups of R-4′-Formamidobenzo-18-Crown-6 ether [21]. Finally, the obtained adsorbent particles were collected by the magnetic method and dried in a vacuum oven. The design and praparation procedure of magnetic adsorbent are illustrated in Fig. 1.

2.2. Characterization of adsorbents

Powder XRD patterns of the specimens were obtained on a PANalytical Empyrean diffractometer with Cu Kα radiation. The shape of the particles were observed using SEM on a LEO 1530VP microscope. High resolution TEM (HRTEM) images and selected area electron diffraction (SAED) patterns were recorded on a JEOL-2011FEF microscope operated at 200 kV. Fourier transform infrared (FTIR) spectra were recorded on a Spectrum One-B FTIR spectrometer with KBr pellets (Perkin Elmer, USA). A Pvris Diamond TGA instrument was used for thermogravimetric (TG)

analysis from 25 °C to 800 °C with a heating ramp of 10 °C in nitrogen gas. The vibrating sample magnetometer (VSM) (PPMS-9T, Quantum Design) was used to obtained the magnetic property of the sample.

2.3. Cs^+ adsorption

The batch adsorption experiments were performed by adding 0.1 g adsorbent into 50 mL of solution of different concentrations of Cs^+ in an 150 mL flask with a shaking speed of 120 rpm. The pH value was adjusted by HCl (1.0 M) and NaOH (1.0 M). 100 ml of 0.1 M NH_4Cl was used for Cs^+ to reach desorption equilibrium in 4 h from adsorbents. A GBC-908 Atomic Absorption Spectrometer (GBC Scientific Equipment Pty Ltd.) was used for testing the concentrations of Cs^+. The Cs^+ removal efficiency (E %) and the adsorption capacity in equilibrium (q_e, mg/g) were calculated using the equations as shown below [22]:

$$E(\%) = \frac{C_0 - C_t}{C_0} \times 100\% \qquad (1)$$

$$q_e = \frac{(C_0 - C_t)V}{m} \qquad (2)$$

where C_0 (mg/L) and C_t (mg/L) are the initial Cs^+ concentration in the solution and that at a given time, m (g) represents the quantity of the adsorbent, and V (L) is the volume of the Cs^+ solution.

2.4. DFT calculations

R-4′-Formamidobenzo-18-Crown-6, on the surface of Fe_3O_4 particles, acted as a receptor of Cs^+ cations. To simplify the description, we use a short term of Fe_3O_4@18-Crown-6 for the final adsorbent. The calculation of the effect of different crown size on chelating Cs^+ was based on the crown ether groups only. However, only 4′-Formamidobenzo-18-Crown-6 was considered in the calculation of chelating different cations. The local structure, stability and electrostatic potential (ESP) of the functional

6

groups chelating the Cs^+ cations were obtained using the wB97XD method reported by Chai and Head−Gordon [23], where def2-TZVP basis set was used for the selected atoms [24,25]. Vibrational frequency calculation was used at the same level to confirm the nature of the stationary points. Basis Set Superposition Error (BSSE) correction was involved partitioning the complex into two fragments *i.e.* Cs^+ and 4'-Formamidobenzo-18-Crown-6. All geometry optimisations and frequency analyses were carried out by the Gaussian 16 software [26].

The interaction between Cs^+ and 4′-Formamidobenzo-18-Crown-6 was measured as the interaction energy (ΔE) and is defined using the equation below:

$$\Delta E = E_{complex} + BSSE - E_{Cs^+} - E_{receptor} \tag{3}$$

where the energy parameters $E_{complex}$, E_{Cs^+}, and $E_{receptor}$ represent to the energy of the complex, Cs^+ and 4'-Formamidobenzo-18-Crown-6, respectively.

Multiwfn program was used for the quantitative analyses (ESP) and average local ionization energy with the grid spacings of 0.15 Bohr [27]. The VMD 1.9 program was employed to render the color ESP and reduced density gradient (RDG) [28,29].

3. Results and Discussion

3.1. Specimen characterization

The prepared adsorbent specimens were initially characterized by using powder XRD. Fig. 2 shows the XRD pattern of the final Fe_3O_4@18-Crown-6 adsorbent. The 2θ values of the diffraction peaks correspond to the d-spacings of the face-centred cubic spinel structure of Fe_3O_4 (JCPDS: 86-1354). It has been noted there is an extra peak at 2θ of 37.38°, which cannot be indexed to the Fe_3O_4 structure. It is unlikely from hematite Fe_2O_3, a common impurity in magnetite Fe_3O_4, since the closest peak from hematite is (110) at 35.61° with a significant difference with 37.38°. In addition, if this peak is from hematite, the strongest peak, (104), at 33.15° should also appear, which is

7

actually absent from our XRD pattern. Fortunately, this small amount of unknown impurity did not significantly affect our adsorption results.
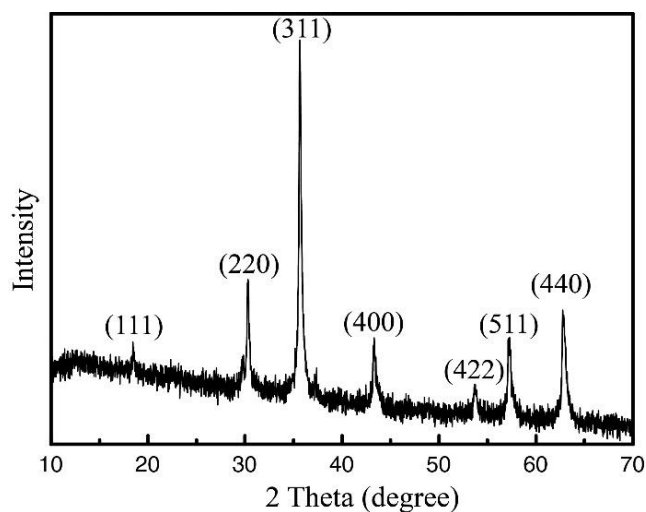

Fig. 2. XRD pattern of the obtained Fe_3O_4@18-Crown-6 adsorbent. The peaks are indexed to the face-centered cubic Fe_3O_4 structure.
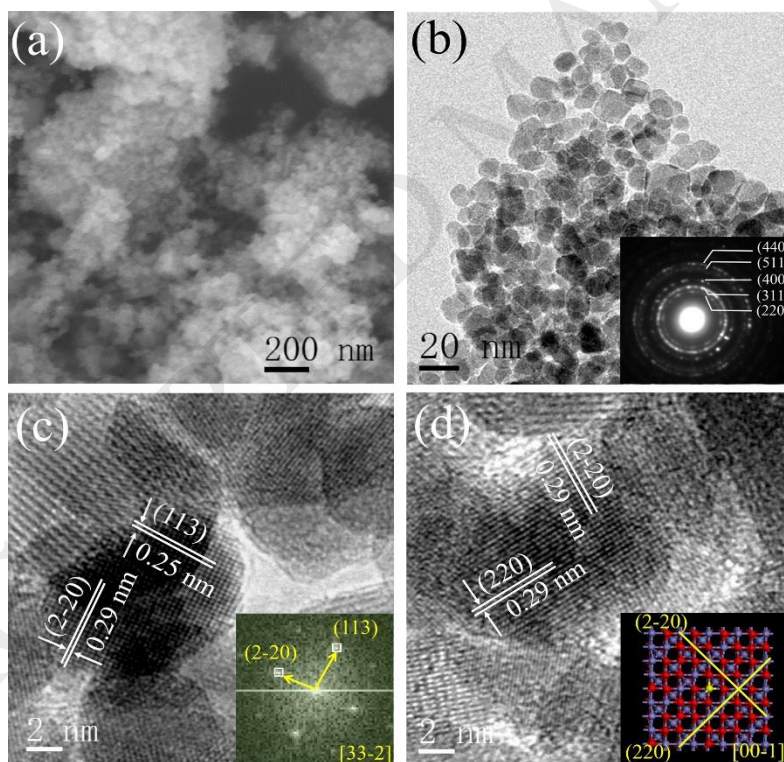

Fig. 3. (a) SEM, (b) TEM and (c, d) HRTEM images of Fe_3O_4@18-Crown-6. The insets are the corresponding (b) SAED pattern, (c) FFT of the image of the central particle, and (d) structural model on the $[00\bar{1}]$ projection.

The size and morphology of the adsorbents were revealed by SEM and TEM (Fig. 3a, 3b), showing a round shape with an average diameter of the particles around 12 nm with a narrow size distribution. The inset in (b) shows a SAED pattern from an area covering many particles. The group of concentric circles corresponds to a series of d-spacings of Fe_3O_4. HRTEM was used to further confirm the Fe_3O_4 structure as shown in Fig. 3c and 3d. From these images, the measured d-spacings, 0.25 and 0.29 nm, can be indexed onto the (113) and ($2\bar{2}0$) planes of the Fe_3O_4 structure, respectively. All the Fe_3O_4 particles have a high crystallinity and are stable under electron beam irradiation even their surface may be covered by an organic layer.
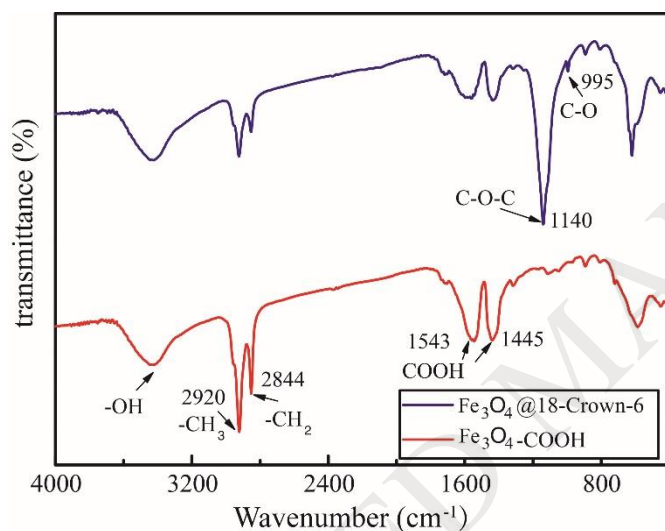

Fig. 4. FTIR spectra of the as-prepared $Fe_3O_4@R-COOH$ and $Fe_3O_4@18$-Crown-6 adsorbent.

Typical FTIR spectra of the precursor $Fe_3O_4@R-COOH$ and the final adsorbent $Fe_3O_4@18$-Crown-6 were used to identify the organic groups presented in the specimens as shown in Fig. 4. The wide band at 3130–3630 cm^{-1} are from the O–H vibrations in the adsorbed water. The obvious peaks at 2920 and 2844 cm^{-1} can be assigned to the $-CH_3$ stretching and the $-CH_2$ stretching modes. The asymmetric and symmetric COO– stretches present at 1543 and 1445 cm^{-1}, indicating that a bidentate fashion comes from the oleic acid chain with two oxygen atoms coordinated symmetrically to the particle surface [30]. Both water and oleic acid present in $Fe_3O_4@R-COOH$ and $Fe_3O_4@18$-Crown-6 adsorbent. The strongest peak around 1140

9

cm^{-1} from Fe_3O_4@18-Crown-6 adsorbent is assigned to the stretching vibration of C–O–C, and the small vibration peak at 995 cm^{-1} is due to the C–O vibration, indicating that the 18-Crown-6 functional groups are at the particle surface [31].
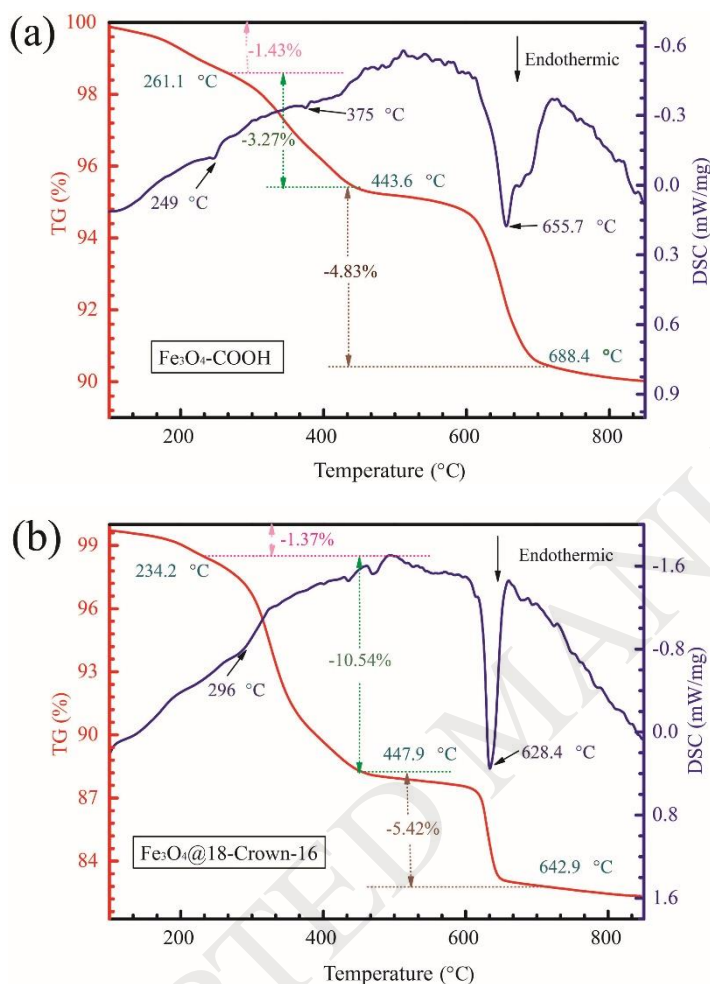

Fig. 5. TG analysis of the as-prepared (a) Fe_3O_4@R–COOH and (b) Fe_3O_4@18-Crown-6 adsorbent.

The thermal stability and degradation processes of Fe_3O_4@R–COOH and Fe_3O_4@18-Crown-6 were studied by TGA. Fig. 5 presents the TGA thermogram of the total weight loss of these particles about 9.53% and 17.33% in a range of temperature from 100°C to 700°C. These weight losses represent three thermal degradation steps. The first weight loss in the low-temperature region (below 260°C) results from the removal of physically and chemically adsorbed water. The weight losses in the second step, from ~260°C to ~450°C, could be attributed to the decomposition of oleic acid

10

adsorb on the Fe$_3$O$_4$@R–COOH surface (3.27% in Fig. 5a) and the decomposition of 18-Crown-6 groups in Fe$_3$O$_4$@18-Crown-6 (10.54% in Fig. 5b). The third step (4.83% in Fig. 5a and 5.42% in Fig. 5b) in a temperature range from 600°C to 700°C, could be attributed to the decomposition of the remained hydrocarbon fragments. Assuming the Fe$_3$O$_4$ particle size is 12 nm in diameter, the TGA results mean that the density of the surface oleic acid molecules is about 1.1/nm^2 in Fe$_3$O$_4$@R–COOH, while the ratio of ether to acid in Fe$_3$O$_4$@18-Crown-6 is about 1 : 1.

3.2. Adsorption studies

3.2.1. Effect of pH values

The initial pH value of the solution has an influence on the Cs$^+$ adsorption on Fe$_3$O$_4$@18-Crown-6. In this study, the initial pH values changed from 1 to 11 were investigated and the results are presented in Fig. 6. The efficiency of adsorption increases rapidly from 50.6% to 97.3% as the pH value increased from 3 to 7, and then decreases gradually to 90.6% with a further increase of pH value from 7 to 11. Low adsorption capacity in acidic environments can be ascribed to the competition of H$^+$ with Cs$^+$ ions at the surface of the crown ether groups. Under alkali condition, the increased ionic strength may affect the adsorption capacity to a certain extent [32].
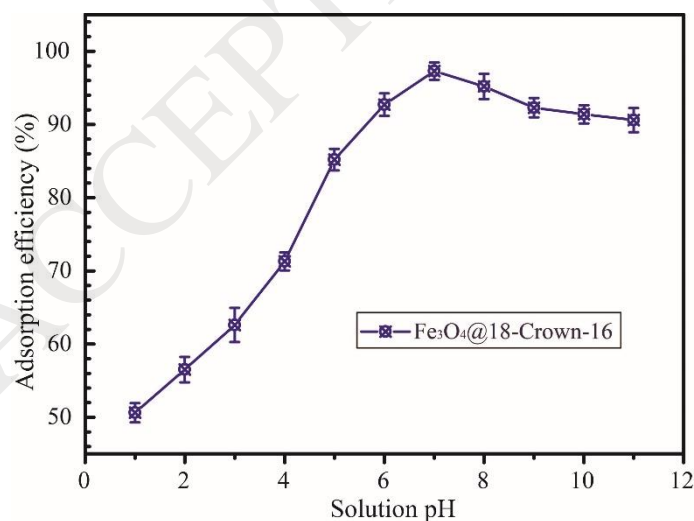

Fig. 6. The influence of initial pH values on the Cs$^+$ adsorption. (C_{Cs+}: 25 mg/ L, adsorbent C_{Ads}: 2.0 g/L, shaking speed r_s: 120 rpm, time t: 150 min, temperature T: 25°C.)

The pH values of the solutions after adding the adsorbent for 5 min and for 4 h were also measured and no change was observed. Cyclic voltammograms (CV) method was used to detect the Fe^{2+} in the solutions after adsorption for 3 h. No obvious Fe^{2+} peak was detected, indicating a high stability of Fe_3O_4 nanocrystallites during the adsorption even in solutions with a low pH.

3.2.2. Adsorption isotherms

In order to describe and understand the adsorption process, the Langmuir and Freundlich isotherms models were used to fit the sorption data [33]:

$$\frac{C_e}{q_e} = \frac{1}{q_m b} + \frac{C_e}{q_m} \qquad (4)$$

$$\ln q_e = \ln k_F + \frac{1}{n} \ln C_e \qquad (5)$$

where C_e (mg/L) is the concentration of Cs^+, q_e (mg/g) is the experimental data of the adsorbed Cs^+ at equilibrium, q_m (mg/g) is the calculated adsorption capacity, b (L/mg) and k_F (mg/g) are the Langmuir and the Freundlich constants, n indicates the adsorption intensity which marked the Freundlich exponent.

Fig. 7 and Table 1 show the data of the Langmuir and Freundlich isotherms models, which are applied for monolayer and multilayer adsorption on the surface. At different temperatures, the Cs^+ adsorption process fits better with the Langmuir isotherm model by higher correlation coefficients R^2, indicating that Cs^+ ions are adsorbed solely on the surface of Fe_3O_4@18-Crown-6 adsorbents by a monolayer adsorption process. From Table 1, the adsorption capacity obtained for Fe_3O_4@18-Crown-6 adsorbent was 26.98 mg/g for Cs^+, which was higher than that reported solid humic acid adsorbent and many inorganic materials in Table S1 [34].
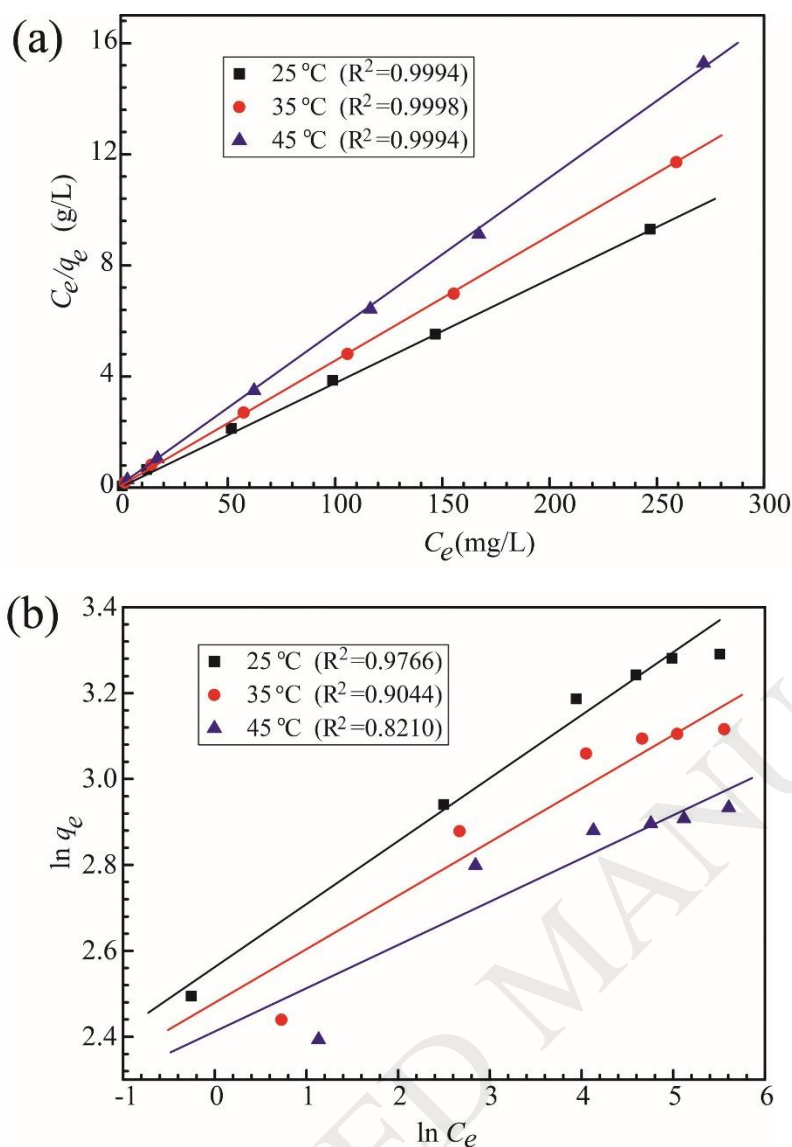
Fig. 7. (a) Langmuir and (b) Freundlich isotherm models for the Cs$^+$ adsorbed onto the Fe$_3$O$_4$@18-Crown-6 adsorbent at different temperatures. (Adsorbent C_{Ads}: 2.0 g/L, shaking speed r_{sh}: 120 rpm).

Table 1. The results of the Langmuir and Freundlich models present for the Cs$^+$ adsorbed onto the Fe$_3$O$_4$@18-Crown-6 adsorbent.

	Langmuir model			Freundlich model		
T (^{o}C)	q$_m$ (mg/g)	b (L/mg)	R^2	k$_F$((mg/g)(L/mg)$^{1/n}$)	n	R^2
25	26.98	0.2569	0.9994	12.9314	6.9161	0.9766
35	22.45	0.3897	0.9998	11.1629	8.7336	0.9044
45	18.01	1.3769	0.9994	10.5369	8.7997	0.8210

3.2.3. Adsorption kinetics

In order to investigate the adsorption mechanism of Cs^+ onto Fe_3O_4@18-Crown-6, the pseudo-first-order and pseudo-second-order kinetic models are used to estimate the adsorption behavior. The corresponding equations are given below:

$$\ln(q_e - q_t) = \ln q_e - k_1 t \qquad (6)$$

$$\frac{t}{q_t} = \frac{1}{k_2 q_e^2} + \frac{t}{q_e} \qquad (7)$$

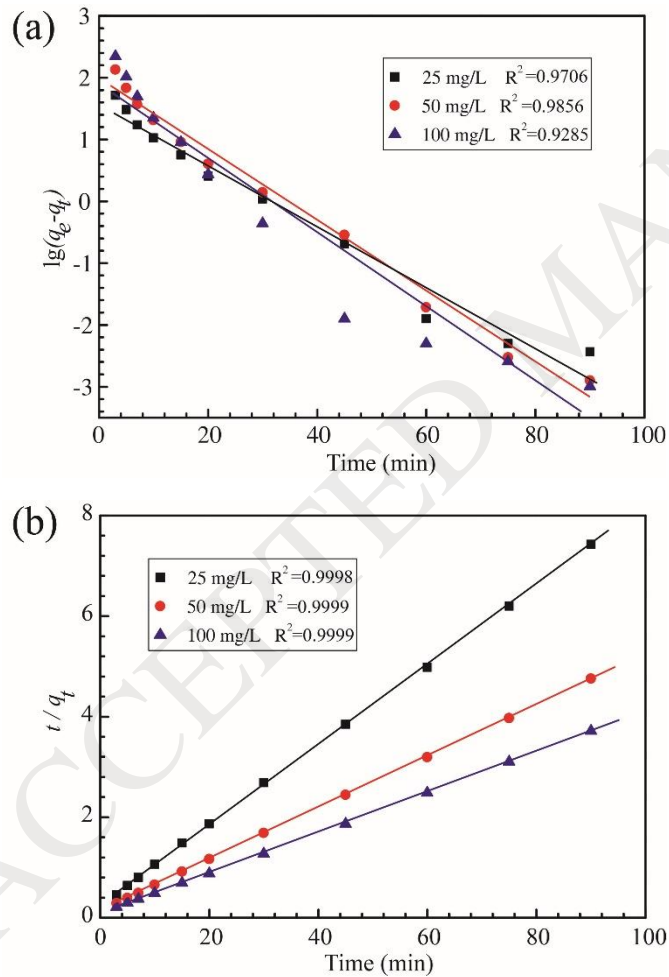**Fig. 8**. (a) Pseudo-first-order and (b) pseudo-second-order kinetics plots for the Cs^+ adsorption on Fe_3O_4@18-Crown-6 at different Cs^+ concentrations. (Adsorbent used C_{Ads}: 2.0 g/L, shaking speed r_{sh}: 120 rpm, temperature T: 25°C)

where q_e and q_t are the adsorption abilities of Cs^+ ions at equilibrium and at a testing time t (min), the equilibrium rate constants in the pseudo-first-order and pseudo-second-order kinetic models are signed as k_1 (1/min) and k_2 (g/(mg min)). The fitting results are shown in Fig. 8.

The fitting kinetic data with the coefficients (R^2) are given in Table 2. The R^2 values of the pseudo-second-order model match better compared to the parameters obtained by the pseudo-first-order model. The experimental capacity values ($q_{e,\exp}$) of adsorption fit well with the calculated values ($q_{e,cal}$) by the pseudo-second-order model. These results suggest that the Cs^+ adsorption behavior can be regarded as chemical adsorption on the active sites of the adsorbent.

Table 2. The pseudo-first-order and pseudo-second-order models match for the Cs^+ adsorption behavior on Fe_3O_4@18-Crown-6 adsorbent.

C_0 (mg/L)	$q_{e.exp}$ (mg/g)	Pseudo-first-order			Pseudo-second-order		
		$q_{e.cal}$ (mg/g)	k_1 (1/min)	R^2	$q_{e.cal}$ (mg/g)	k_2 (g/mg min)	R^2
25	12.20	4.8105	0.0499	0.9706	12.5834	0.0260	0.9998
50	18.98	7.1578	0.0577	0.9856	19.5465	0.01991	0.9999
100	24.25	7.0600	0.0635	0.9285	24.9128	0.01975	0.9999

The rate-limiting step of the adsorption process was investigated by the Weber Morris surface diffusion model. Usually, there are three consecutive steps in the Cs^+ adsorption process: (1) Cs^+ ions transfer from solution onto the exterior adsorbent surface; (2) Cs^+ ions on the particle surface transport to the 18-Crown-6 functional groups; (3) exchange the adsorbed Cs^+ ions between the particle surface and the solution (equilibrium steps). The intra-particle diffusion model is given as below:

$$q_t = k_n t^{0.5} + C_n \qquad (8)$$

where q_t (mg/g) is the adsorption at a testing time, k_n (mol g^{-1} min$^{-0.5}$) is the diffusion rate constant in the adsorption process of different steps (n = 1 to 3). The lines of q_t vs $t^{0.5}$ of Fe$_3$O$_4$@18-Crown-6 adsorbents and the k_1, k_2 and k_3 values obtained from the plots are shown in Fig. 9a. The first linear portion of the lines has a steep slope, indicating the important controlling step is the diffusion of the ions to the particle surface or the liquid-solid interface. It is the initial fast kinetics feature. A less steep slope in the second linear part represents a gradual migration of Cs$^+$ ions from the particle surface to the side of crown ether groups, indicating a slow kinetics feature. The intra-particle diffusion further slows down and the adsorption of Cs$^+$ ions approaches to an equilibrium state in the third linear stage.
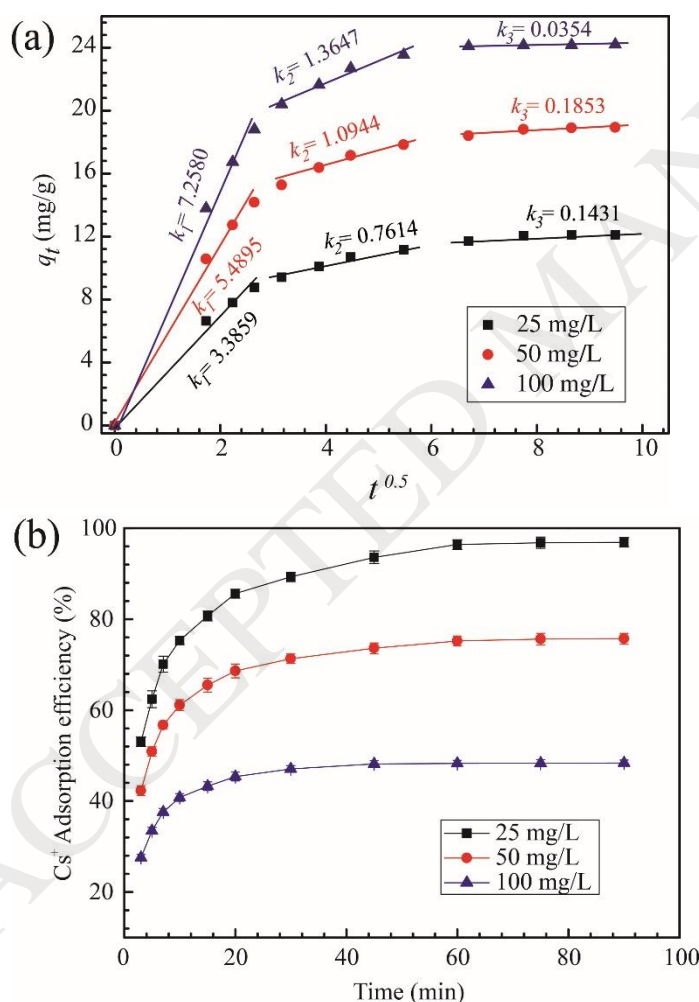

Fig. 9. (a) The intra-particle diffusion modelling of Cs$^+$ adsorption on the Fe$_3$O$_4$@18-Crown-6 adsorbent. (b) Effect of experimental time on Cs$^+$ adsorption at different initial concentrations. (Adsorbent used C_{Ads}: 2.0 g/L, shaking speed r_{sh}: 120 rpm, temperature T: 25°C).

Fig. 9b shows the adsorption of the Fe_3O_4@18-Crown-6 adsorbent for Cs^+ in solutions with different Cs^+ concentrations of 25, 50, and 100 mg/L as a function of time. As shown in the figure, the Cs^+ cations are adsorbed onto the particle surface quickly, and reaches to equilibrium within 30 min when the initial concentration of Cs^+ is 100 mg/L. Since 0.1 g adsorbent can remove 2.425 mg Cs^+ in 50 ml solution, the removal percent is 48.5 %. This relatively low percent ensures a quick approach to the equilibrium, allowing us to obtain the maximum adsorption, or an approximate adsorption capacity, which is 24.25 mg/g.

When the concentration of Cs^+ decreases to 50 mg/L in the solution, the percent of removal in 90 min increases to 75.92%. The total amount of Cs^+ removed is 18.98 mg/g, which is lower than the maximum capacity of the adsorbent. Kinetic factors seem to control the further adsorption. In other words, it would take longer time to approach the equilibrium state. In a Cs^+ solution of 25 mg/L, the percent of Cs^+ removal further increases to 96.9% at 90 min. The remaining Cs^+ in the solution is 0.775 mg/L. Again, at this moment, only about 50% of the capacity of the adsorbent have been used. The remaining 50% active sites can potentially further adsorb Cs^+ with the adsorption rate controlled kinetically.

3.2.4. Adsorption selectivity

One of the important problems that restricts applications of the sorption method in extracting desired ions is the ion selectivity of the sorbent. The most challenging work is to perform ion separation of Cs^+ from natural water in a salt lake or wastewater, in which multiple types of ions result in a high ionic strength and become competitive ions during the adsorption. In fact, cesium often coexists with other alkali ions such as Li^+, Na^+ and K^+ in aqueous solutions.
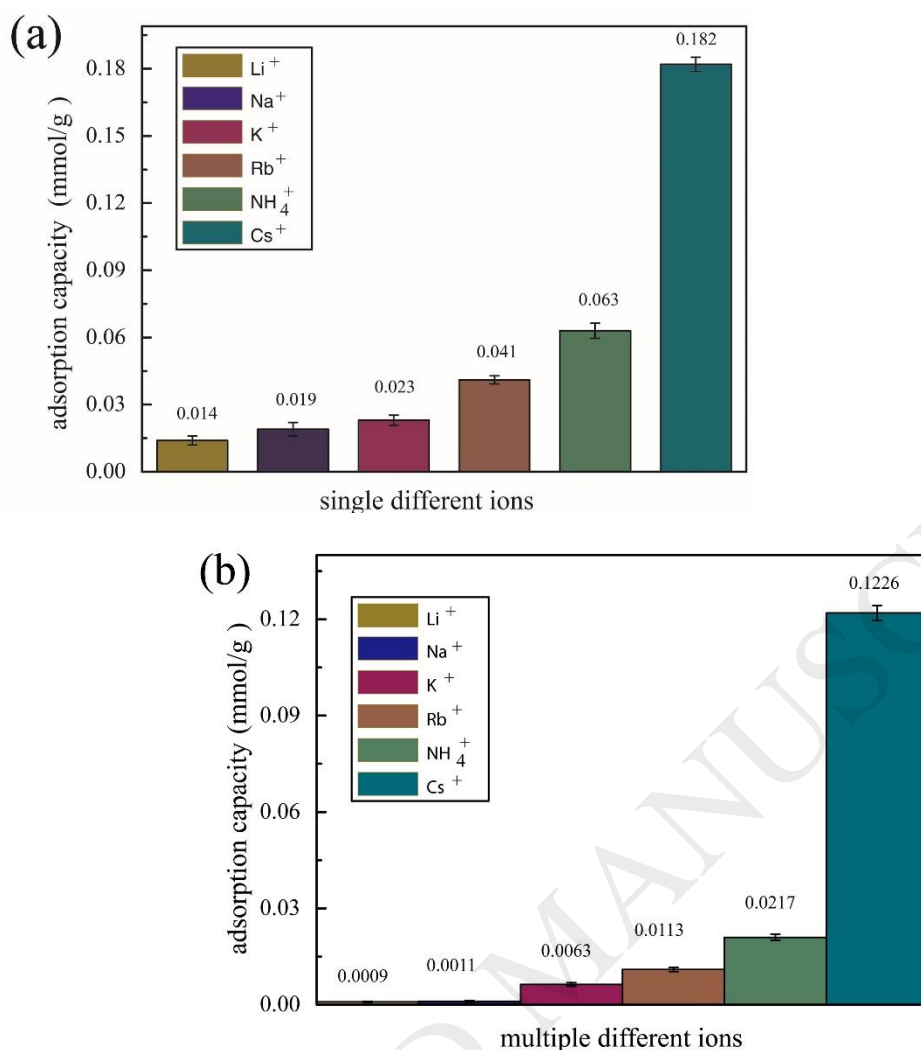
Fig. 10. Equilibrium adsorption capacities of Fe_3O_4@18-Crown-6 adsorbent in the (a) non-competitive solutions with 0.75 mmol/L in each solution; and (b) a competitive solution with 0.75 mmol/L for each cation. The total concentration of the all six cations in the latter is therefore 4.5 mmol/L.

Fig. 10 illustrates the adsorption ability of the Fe_3O_4@18-Crown-6 adsorbent for Cs^+ in presence of different cations (Li^+, Na^+, K^+, Rb^+, NH_4^+). The maximum adsorption abilities are in order of $Cs^+ > NH_4^+ > Rb^+ > K^+ > Na^+ > Li^+$ in both the non-competitive and competitive adsorption conditions, and this order is like the order of ionic diameters in Table S2. It is shown that the non-competitive adsorption abilities in single alkali metal ions are better than the ions coexist systems by the influence of stronger ionic strength. This affects the adsorption ability by decreasing ~32.6%. On the other hand, the relative Cs^+ adsorption capacity was not influenced significantly by the presence of NH_4^+, Rb^+,

18

K^+, Na^+ and Li^+ ions in the solution. The prepared adsorbent presents favorable selectivity for Cs^+, especially in the systems with multiple ions. This is because the target Cs^+ ions are impregnated into the holes of 18-Crown-6 with a suitable ionic size, while the co-existing cations (NH_4^+, Rb^+, K^+, Na^+ and Li^+) have smaller ionic radii than Cs^+, leading to some difficulties to form stable chelated structures. Consequently, Fe_3O_4@18-Crown-6 has a high affinity for Cs^+ ions and indeed is an effective adsorbent for Cs^+ in aqueous solutions.

3.3 Magnetic separation property and recycling

Reusability is crucially important to evaluate the adsorbent's performance because of the economic and environmental considerations in many applications. In the present work, the adsorbent underwent ten consecutive adsorption/desorption cycles, where 50 mL of 25 mg/L Cs^+ solution was used in the adsorption step, while 100 mL of 0.1 M NH_4Cl was used as desorbing agent in the desorption. Each of them was shaken for 4 h at 25 ˚C, and the adsorbent was collected by a magnet after desorption. As shown in Fig. 11, the Cs^+ adsorption ability presents a slow downward trend with increasing the cycle numbers to ten, from 94.3% to 86.4%. At the end of the tenth cycle, the Fe_3O_4@18-Crown-6 adsorbent retained more than 90% of its original Cs^+ adsorption capacity, and >85% of the total adsorbed Cs^+ can be eluted during the desorption steps. This high stability indicates that the 18-Crown-6 functional group has firmly coated on the Fe_3O_4 surface.

The magnetic property of the Fe_3O_4@18-Crown-6 adsorbent has also been investigated (Fig. 12). The magnetizations at the applied magnetic field of 2500 Oe can reach to 78.7 emu/g, implying a strong magnetic response to the magnetic field. The remanence of the Fe_3O_4@18-Crown-6 adsorbent is 0.41 emu/g, and the corresponding coercivity is 4.2 Oe. This adsorbent possesses low remanent magnetization and low coercivity, indicating a superparamagnetic property. The magnetic curve shows non-linear, reversible characteristic and low hysteresis, indicating a good magnetic separation ability.
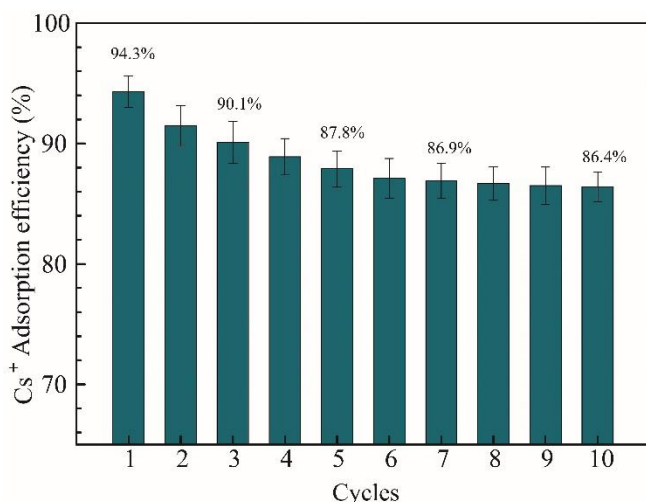
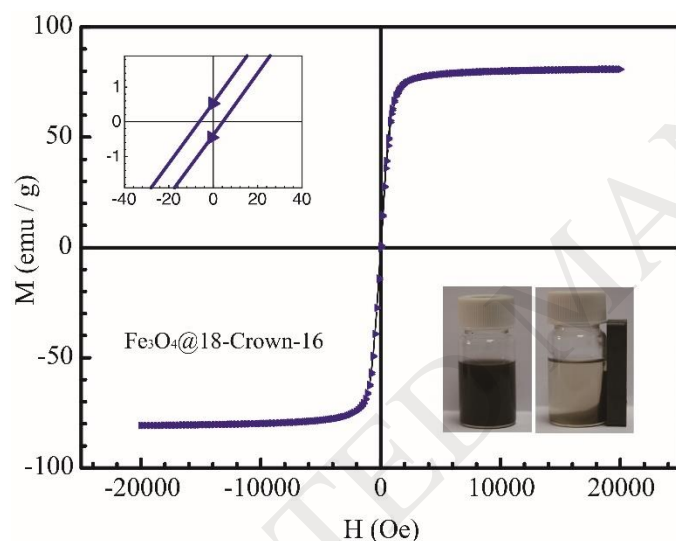**Fig. 11.** Percentage of Cs⁺ removal by Fe₃O₄@18-Crown-6 adsorbent during ten adsorption/desorption cycles.

Fig. 12. Hysteresis curves of Fe₃O₄@18-Crown-6 adsorbent measured at room temperature.

3.4. DFT calculations of the adsorbent surface structure

The selectively chelating cations is governed by the structure of the crown ether. We optimized the ring size of crown ethers to fit with Cs⁺ ions by the theoretical quantum mechanical DFT calculations (Fig. S1). From the calculated results, the ring sizes of 21-Crown-7 and 24-Crown-8 are too big to house a Cs⁺ ion in a symmetric manner. The crown ether backbone likes to distort near the Cs⁺ cation in a tendency of lowering the symmetry to reduce energy. The 15-Crown-5 is also unstable when

20

chelating with a Cs^+ ion, leading to a serious structural distortion. So the above three crown ethers have difficulties in chelating Cs^+ to form a symmetric coordination. On the other hand, the 12-Crown-4 has a stable structure with Cs^+ by forming four symmetric coordinated bonds, but the binding ability is lower than 18-Crown-6 chelated with Cs^+ in six symmetric coordination. Furthermore, a smaller ring size of 12-Crown-4 may reduce the selectivity for Cs^+. The above calculations suggest that the chelated structure largely depends on the different sizes of crown ethers, and the selective adsorption ability is strongly influenced by the symmetry of coordination structure and binding energy. This calculation guided us to select 18-Crown-6 as the functional component in the adsorbent in the present work.

The selectivity of ions adsorbed on 18-Crown-6 is also important to be concerned. We present the DFT study of the interaction between 4′-formamidobenzo-18-Crown-6 and different alkali cations (H^+, Li^+, Na^+, K^+, Rb^+, Cs^+ and NH_4^+) by evaluating the geometries and binding energies (Fig. 13). The calculations clearly show that 4′-formamidobenzo-18-Crown-6 chelated with H^+, Li^+ and Na^+ are seriously distorted from six coordination symmetry, because these cations are too small to fill the cavity. Their binding energies are bigger than others due to that the crown ether would distort by losing the high symmetry. The 4′-formamidobenzo-18-Crown-6 offers six coordination to K^+, Rb^+, Cs^+ and NH_4^+ and keep a good symmetry when the cavity is fully occupied [35]. Among them, Cs^+ binding with crown ether has a lower energy ($\Delta E = -70.02\ kcal/mol$) than K^+, Rb^+ and NH_4^+, indicating that the binding between crown ether and Cs^+ is significantly stronger. We suspect that adding water molecules to these complexes will further stabilize the structures. But we anticipate that this selectivity sequence would be unchanged.
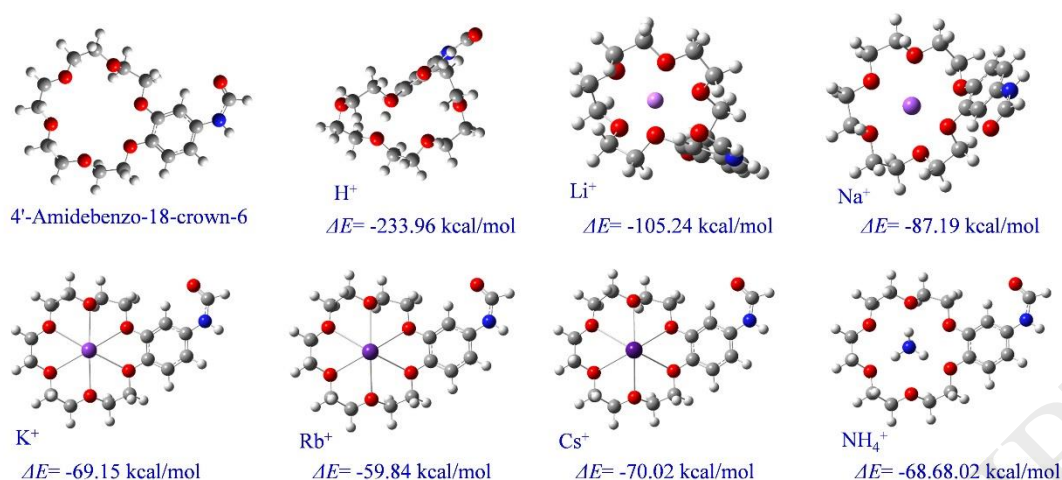
Fig. 13. Top view of the DFT optimized structures of the different alkali metal cations chelated by 4'-formamidobenzo-18-Crown-6.
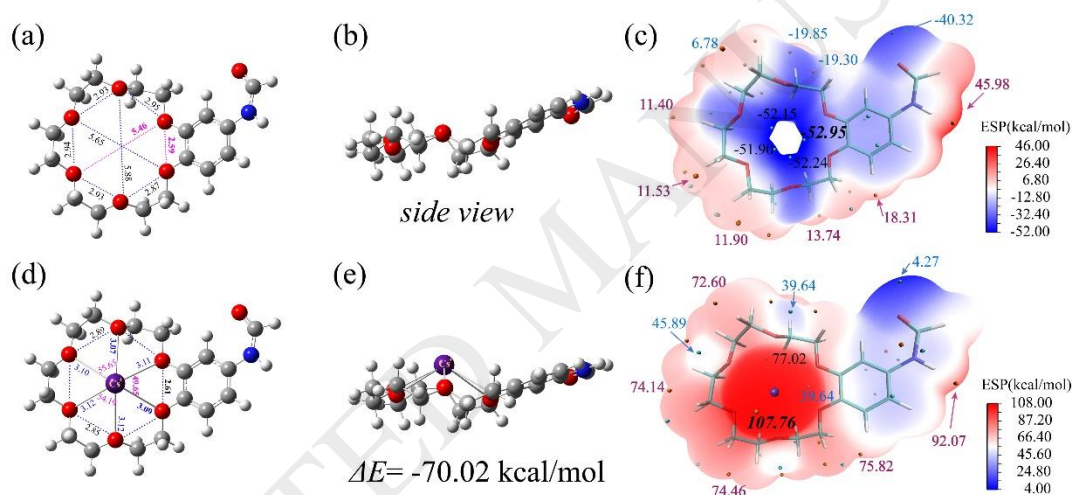

Fig. 14. DFT optimized structures of 4'-formamidobenzo-18-Crown-6 molecules with and without chelating Cs^+. (a), (b) Top and side views of the molecule. (d), (e) Top and side views of the molecule after Cs^+ is chelated. (c), (f) ESP mapping of the molecule before and after Cs^+ is adsorbed.

To further study the surface structure of the Fe_3O_4@18-Crown-6 adsorbent, DFT calculations were employed for the 18-Crown-6 functional group structures chelating with Cs^+ ions. We firstly optimized the molecular geometries of the 18-Crown-6 functional group in calculations and illustrated in Fig. 14a,b.

The electrostatic potential mapping of the adsorbent surface is usually used to study the reactivity of the adsorbent. A site with more negative electrostatic potential will

own the stronger ability to attract electrophiles and it's more likely to act as the active site (Fig. 14c and Fig. S2–S5). The distance between the two oxygen atoms that beside the benzene is shorter (2.59 Å) than the inter-atomic distances of other four oxygen atoms, resulting in a site possessing the most negative electrostatic potential near the benzene ring (−52.95 kcal/mol). There are four sites in total owning more negative electrostatic potential (−51.90, −52.15, −52.24 and −52.95 kcal/mol). We calculated a Cs^+ ion approaching to these four sites by the DFT optimization. The structure of the Cs^+ chelated on 18-Crown-6 surface with the corresponding bond lengths is depicted in Fig. 14d,e. From these pictures, binding with the Cs^+ cation changes the structure of the 18-Crown-6 moiety slightly. This type of calculated cationic complex structure, which is most energetically favored, has a ''central'' cation Cs^+ chelated by strong bonds to six oxygen atoms from the respective 18-Crown-6 moiety (3.11, 3.09, 3.12, 3.12, 3.10, and 3.07 Å).

As the Cs^+ is adsorbed, the positive electrostatic potential of the site near the ''crown center'' reaches 107.76 kcal/mol, indicating that other anions such as Cl^-, SO_4^{2-}, H_2O etc. would attach to this site [36,37]. Finally, the interaction energy (ΔE) of the Cs^+ adsorbed on Fe_3O_4@18-Crown-6 was found to be −70.02 kcal/mol, which indicates that the adsorption process is an exothermic chemical reaction [38], showing a very good agreement with experimental results.

4. Conclusions

In this study, we have prepared a magnetic Cs^+ adsorbent by attaching 18-Crown-6 functional groups to the surface of Fe_3O_4 nanoparticles. In order to obtain relevant data about the chelating interactions between the 18-Crown-6 moiety and the Cs^+ ions, adsorption experiments and theoretical DFT calculations were performed. The adsorption efficiency of this adsorbent can reach to 96.9% in 25 mg/L Cs^+ solution without pH adjustment. Besides this, it owns fast adsorption by achieving the maximum adsorption, high Cs^+ adsorption selectivity and much fast 'green' magnetic separation ability. The present work implies that Fe_3O_4@18-Crown-6 is a promising adsorbent for

Cs^+ extraction from wastewater, and the methodology may be applied to extract other useful ion resources from salt lakes and seawater.

Acknowledgements

Conflicts of interest
There are no conflicts to declare.

References

[1] S.M. Husnain, W. Um, Y.Y. Chang, Y.S. Chang, Recyclable superparamagnetic adsorbent based on mesoporous carbon for sequestration of radioactive cesium, Chem. Eng. J. 308 (2017) 798−808.

[2] H. Kim, M. Kim, W. Lee, S. Kim, Rapid removal of radioactive cesium by polyacrylonitrile nanofibers containing Prussian blue, J. Hazard Mater. 347 (2018) 106−113.

[3] A.Y. Zhang, Q.H. Hu, Removal of cesium by countercurrent solvent extraction with a calix[4]crown derivative, Sep. Sci. Technol. 52 (2017) 1670−1679.

[4] H. Deng, Y.X. Li, L. Wu, X. Ma, The novel composite mechanism of ammonium molybdophosphate loaded on silica matrix and its ion exchange breakthrough curves for cesium, J. Hazard Mater. 324 (2017) 348−356.

[5] N. Paul, R.B. Hammond, T.N. Hunter, M. Edmondson, L. Maxwell, S. Biggs, Synthesis of nuclear waste simulants by reaction precipitation: Formation of caesium phosphomolybdate, zirconium molybdate and morphology modification with citratomolybdate complex, Polyhedron 89 (2015) 129−141.

[6] Z.Q. Jia, X.X. Cheng, Y.X. Guo, L.Y. Tu, In-situ preparation of iron(III)

hexacyanoferrate nano-layer on polyacrylonitrile membranes for cesium adsorption from aqueous solutions, Chem. Eng. J. 325 (2017) 513−520.

[7] R.D. Ambashta, D.S. Deshingkar, P.K. Wattal, D. Bahadur, Application of magnetite hexacyanoferrate composites in magnetically assisted chemical separation of cesium, J. Radioanal. Nucl. Chem. 270 (2006) 585−592.

[8] T. Sasaki, S. Tanaka, Magnetic separation of cesium ion using prussian blue modified magnetite, Chem. Lett. 41 (2012) 32−34.

[9] O.A.A. Moamen, H.A. Ibrahim, N. Abdelmonem, I.M. Ismail, Thermodynamic analysis for the sorptive removal of cesium and strontium ions onto synthesized magnetic nano zeolite, Micropor. Mesopor. Mat. 223 (2016) 187−195.

[10] A. Patel, R. Sadasivan, Microwave assisted one pot synthesis and characterization of cesium salt of di-copper substituted phosphotungstate and its application in the selective epoxidation of cis-cyclooctene with tert-butyl hydroperoxide, Inorg. Chim. Acta 458 (2017) 101−108.

[11] K. Qin, F. Li, S. Xu, T.H. Wang, C.H. Liu, Sequential removal of phosphate and cesium by using zirconium oxide: A demonstration of designing sustainable adsorbents for green water treatment, Chem. Eng. J. 322 (2017) 275−280.

[12] D. Parajuli, A. Takahashi, H. Noguchi, A. Kitajima, H. Tanaka, M. Takasaki, K. Yoshino, T. Kawamoto, Comparative study of the factors associated with the application of metal hexacyanoferrates for environmental Cs decontamination, Chem. Eng. J. 283 (2016) 1322−1328.

[13] X. Yu, X. Zhang, Y. Meng, Y. Zhao, Y. Li, W. Xu, Z. Liu, CO adsorption, dissociation and coupling formation mechanisms on Fe_2C (001) surface, Appl. Surf. Sci. 434 (2018) 464−472.

[14] M.R. Awual, Ring size dependent crown ether based mesoporous adsorbent for high cesium adsorption from wastewater, Chem. Eng. J. 303 (2016) 539−546.

[15] M.R. Awual, S. Suzuki, T. Taguchi, H. Shiwaku, Y. Okamoto, T. Yaita, Radioactive cesium removal from nuclear wastewater by novel inorganic and conjugate adsorbents, Chem. Eng. J. 242 (2014) 127−135.

[16] S. Sadeghi, F. Fathi, Polymeric membrane coated graphite cesium selective

electrode based on 4',4aEuro(3)(5') di-tert-butyl di-benzo-18-Crown-6, J. Incl. Phenom. Macrocycl. Chem. 67 (2010) 91−98.

[17] Y. Zhang, X.Y. Wang, B.H. Luo, Y. Xia, Density functional theory study of the bis-3-benzo-crown ethers and their complexes with alkali metal cations Na^+, K^+, Rb^+ and Cs^+, J. Phys. Org. Chem. 25 (2012) 222−229.

[18] E. Mei, J.L. Dye, A.I. Popov, Cs-133 nuclear magnetic-resonance study of complexation of cesium tetraphenylborate by 18-Crown-6 in pyridine solutions, J. Am. Chem. Soc. 99 (1977) 5308−5311.

[19] P. Vanura, E. Makrlik, Z. Valentova, Solvent extraction of microamounts of cesium from water into nitrobenzene by using hydrogen dicarbollylcobaltate in the presence of dicyclohexyl-18-Crown-6, Chem. Pap. 57 (2003) 225−228.

[20] X. Liang, X. Wang, J. Zhuang, Y.T. Chen, D.S. Wang, Y.D. Li, Synthesis of nearly monodisperse iron oxide and oxyhydroxide nanocrystals, Adv. Funct. Mater. 16 (2006) 1805−1813.

[21] T. Ito, T. Ikemoto, Y. Isogami, H. Wada, M. Sera, Y. Mizuno, M. Wakimasu, Practical synthesis of low-density lipoprotein receptor upregulator, N-[1-(3-phenylpropane-1-yl)piperidin-4-yl]-5-thia-1,8b-diazaacenaphthylene-4-carboxamide, Org. Process Res. Dev. 6 (2002) 238−241.

[22] Z. Liu, R.T. Yu, Y.P. Dong, W. Li, B.L. Lv, The adsorption behavior and mechanism of Cr(VI) on 3D hierarchical alpha-Fe_2O_3 structures exposed by (001) and non-(001) planes, Chem. Eng. J. 309 (2017) 815−823.

[23] J.D. Chai, M. Head-Gordon, Long-range corrected hybrid density functionals with damped atom-atom dispersion corrections, Phys. Chem. Chem. Phys. 10 (2008) 6615−6620.

[24] F. Weigend, R. Ahlrichs, Balanced basis sets of split valence, triple zeta valence and quadruple zeta valence quality for H to Rn: Design and assessment of accuracy, Phys. Chem. Chem. Phys. 7 (2005) 3297−3305.

[25] C. Mayeux, J. Tammiku-Taul, L. Massi, E.L. Lohu, P. Burk, P.C. Maria, J.F. Gal, Interaction of the cesium cation with mono-, di-, and tricarboxylic acids in the gas phase. A Cs^+ affinity scale for cesium carboxylates ion pairs, J. Am. Soc. Mass Spectrom. 20

(2009) 1912–1924.

[26] M.J. Frisch, G.W. Trucks, H.B. Schlegel, G.E. Scuseria, M.A. Robb, J.R. Cheeseman, G. Scalmani, V. Barone, G.A. Petersson, H. Nakatsuji, X. Li, M. Caricato, A.V. Marenich, J. Bloino, B.G. Janesko, R. Gomperts, B. Mennucci, H.P. Hratchian, J.V. Ortiz, A.F. Izmaylov, J.L. Sonnenberg, D. Williams-Young, F. Ding, F. Lipparini, F. Egidi, J. Goings, B. Peng, A. Petrone, T. Henderson, D. Ranasinghe, V.G. Zakrzewski, J. Gao, N. Rega, G. Zheng, W. Liang, M. Hada, M. Ehara, K. Toyota, R. Fukuda, J. Hasegawa, M. Ishida, T. Nakajima, Y. Honda, O. Kitao, H. Nakai, T. Vreven, K. Throssell, J.A. Montgomery Jr., J.E. Peralta, F. Ogliaro, M.J. Bearpark, J.J. Heyd, E.N. Brothers, K.N. Kudin, V.N. Staroverov, T.A. Keith, R. Kobayashi, J. Normand, K. Raghavachari, A.P. Rendell, J.C. Burant, S.S. Iyengar, J. Tomasi, M. Cossi, J.M. Millam, M. Klene, C. Adamo, R. Cammi, J.W. Ochterski, R.L. Martin, K. Morokuma, O. Farkas, J.B. Foresman, D.J. Fox, Gaussian 16, Gaussian, Inc, Wallingford CT, 2016.

[27] T. Lu, F.W. Chen, Multiwfn: A multifunctional wavefunction analyzer, J. Comput. Chem. 33 (2012) 580–592.

[28] T. Lu, F.W. Chen, Quantitative analysis of molecular surface based on improved marching tetrahedra algorithm, J. Mol. Graph Model 38 (2012) 314–323.

[29] W. Humphrey, A. Dalke, K. Schulten, VMD: Visual molecular dynamics, J. Mol. Graph Model 14 (1996) 33–38.

[30] X. Liang, X. Wang, J. Zhuang, Y.T. Chen, D.S. Wang, Y.D. Li, Synthesis of nearly monodisperse iron oxide and oxyhydroxide nanocrystals, Adv. Funct. Mater. 16 (2006) 1805–1813.

[31] M. Ahmadi, T. Madrakian, A. Afkhami, Solid phase extraction of amoxicillin using dibenzo-18-Crown-6 modified magnetic-multiwalled carbon nanotubes prior to its spectrophotometric determination, Talanta 148 (2016) 122–128.

[32] R. Saberi, A. Nilchi, S.R. Garmarodi, R. Zarghami, Adsorption characteristic of Cs-137 from aqueous solution using PAN-based sodium titanosilicate composite, J. Radioanal. Nucl. Chem. 284 (2010) 461–469.

[33] Z. Liu, R.T. Yu, Y.P. Dong, W. Li, W.Z. Zhou, Preparation of alpha-Fe_2O_3 hollow spheres, nanotubes, nanoplates and nanorings as highly efficient Cr(VI) adsorbents,

RSC Adv. 6 (2016) 82854–82861.

[34] O. Celebi, A. Kilikli, H.N. Erten, Sorption of radioactive cesium and barium ions onto solid humic acid, J. Hazard Mater. 168 (2009) 695–703.

[35] E.D. Glendening, D. Feller, M.A. Thompson, An ab-initio investigation of the structure and alkali-metal cation selectivity of 18-Crown-6, J. Am. Chem. Soc. 116 (1994) 10657–10669.

[36] J.D. Rodriguez, T.D. Vaden, J.M. Lisy, Infrared spectroscopy of ionophore-model systems: hydrated alkali metal ion 18-Crown-6 ether complexes, J. Am. Chem. Soc. 131 (2009) 17277–17285.

[37] Y. Inokuchi, T. Ebata, T.R. Rizzo, O.V. Boyarkin, Microhydration effects on the encapsulation of potassium ion by dibenzo-18-Crown-6, J. Am. Chem. Soc. 136 (2014) 1815–1824.

[38] X. Yu, X. Zhang, X.-W. Yan, Stability of the $Fe_{12}O_{12}$ cluster, Nano Res. 11 (2018) 3574–3581.